ISSN 1569-4410

PHOTONICS AND NANOSTRUCTURES
Fundamentals and Applications

Editors
H. Benisty
T. Krauss
E. Ozbay
C.M. Soukoulis

Volume 9, Issue 1, February 2011

Surface plasmon enhanced IR absorption: Design and experiment

M.S. Shishodia [a], P.V.V. Jayaweera [a], S.G. Matsik [a],
A.G.U. Perera [a,*], H.C. Liu [b], M. Buchanan [b]

[a] *Department of Physics and Astronomy, Georgia State University, Atlanta, GA 30303, USA*
[b] *Institute of Microstructural Sciences, National Research Council, Ottawa, Canada K1A0R6*

Abstract

Metal corrugated surfaces have the potential of enhancing optical absorption through surface plasmon (SP) excitation facilitated by light-metal interactions. The successful utilization of metal corrugation induced optical absorption can improve the response of free carrier absorption (FCA), based HEterojunction Interfacial Workfunction Internal Photoemission (HEIWIP) detectors. This article reports theoretical and experimental investigations of SP-induced infrared (IR) absorption in GaAs based structures, exhibiting absorption peak wavelength (λ_p) in the 10–14 μm region. Moreover, substantial absorption and responsivity improvement using metallic corrugation on typical heterojunction detector is predicted. Proposed design and optimization approaches will be useful for improving the performance of IR detectors.
© 2011 Elsevier B.V. All rights reserved.

Keywords: Photodetectors; IR absorption; Surface Plasmon; Metal corrugation

1. Introduction

Surface plasmons (SPs) [1] have attracted the attention of scientists and engineers involved in a wide arena of research, including data storage, microscopy, diagnostics, and sensing. The advent of nanofabrication tools and technology has provided an increased thrust for exploring the potential of SPs in improving the performance of photonic devices. Inherent momentum mismatch between SP-Photon pairs, due to their dispersion relation requires a momentum tuning device to excite SPs. Metallic corrugation patterned as a periodic grating used for this purpose has been investigated for SP mediated resonant absorption in the visible region for a multilayered plasmonic structure [2], grating optimization for the efficient SP excitation at 633 nm [3] and 476 nm [4], and for designing improved HgCdTe [5] and angled incidence quantum-well infrared photodetectors (QWIPs) [6]. Most of the efforts as described above concentrate on a specific wavelength or a specific detection mechanism. Therefore, these optimization approaches are not suitable for designing SP-coupled heterojunction detectors such as, HEIWIPs operating in the infrared (IR) region. This paper reports: (i) the experimental demonstration and the theoretical corroboration of metal grating-induced optical absorption and the tunability of λ_p in the 10–14 μm region, (ii) absorption and responsivity improvement in FCA-based typical HEIWIP structure through metallic grating antenna, and (iii) the role of structure parameters and the importance of their optimization in spectral tuning and absorption maximization.

* Corresponding author at: Department of Physics and Astronomy, 29 Peachtree Center Avenue, Atlanta, GA 30303-4106, USA.
Tel.: +1 404 413 6037; fax: +1 404 413 6025.
E-mail address: uperera@gsu.edu (A.G.U. Perera).

2. Theoretical model

The structure for present study consists of air, grating, SiO$_2$ and semi-infinite GaAs media, denoted as MED-*j* ($j = 1, 2, 3,$ and 4), and characterized by permittivity (ε_j) and thickness (h_j) is shown in Fig. 1(E). While MED-*j* ($j = 1, 3, 4$) are homogeneous, MED-2 is inhomogeneous and constitutes the metallic corrugation in the form of grating consisting of alternating metallic and open gap regions of widths, a_m and a_g, with permittivity, ε_m and ε_g, respectively. The normal electric field component exciting SPs being zero in s-polarized wave, present analysis is limited to p-polarization. The electromagnetic field (EMF) distribution in this structure is determined using the well-established Modal Expansion Method (MEM) [7,8], where the EMF in MED-2 is theoretically-calculated by expanding the field over numerically-calculated eigenmodes and in the MED-*j* ($j = 1, 3, 4$) is calculated by writing the field as:

$$H^{(j)}(x,z) = \sum_{n=-\infty}^{\infty} \{A_n^{(j)} \exp[i\{k_{xn}x - \kappa_{zn}^{(j)}(z - \tilde{z})\}]$$
$$+ B_n^{(j)} \exp[i\{k_{xn}x + \kappa_{zn}^{(j)}(z - \tilde{z})\}]\},$$

with $\tilde{z} = z_1, z_2, z_3$, The coefficients, $A_n^{(j)}$ and $B_n^{(j)}$, are the amplitudes of the forward and backward propagating wave of order n in *j*th medium. Propagation constants $\kappa_{zn}^{(j)}$ are determined using $\kappa_{zn}^{(j)} = (\varepsilon_j k_0^2 - k_{xn}^2)^{1/2}$, k_{xn}, denoting the in-plane wave vector of the diffraction wave of order *n* ($= 0, \pm 1, \pm 2, \ldots \pm \infty$) and k_0 denoting the magnitude of the incident wave vector. The continuity of the tangential field components at the structure interfaces produce a system of algebraic equations. This system of equations is solved numerically. The number of summation terms in the field expression is iteratively determined by ensuring the convergence of reflection (R) and transmission (T) coefficients. The present analysis is limited to the zeroth order transmission and reflection relevant for the experimental situation [8]. The normalized absorption (N_A) is defined as $N_A = (1 - T - R)/(1 - R)$ [9]. The dielectric function of the metal is calculated using $\varepsilon_m(\omega) = 1 - [\omega_p^2/\omega(\omega + i/\tau)]$, ω_p and τ denoting the plasma frequency and the relaxation time, and their values being, 3.39×10^{15} s^{-1} and 1.075×10^{-14} s, respectively [8,10].
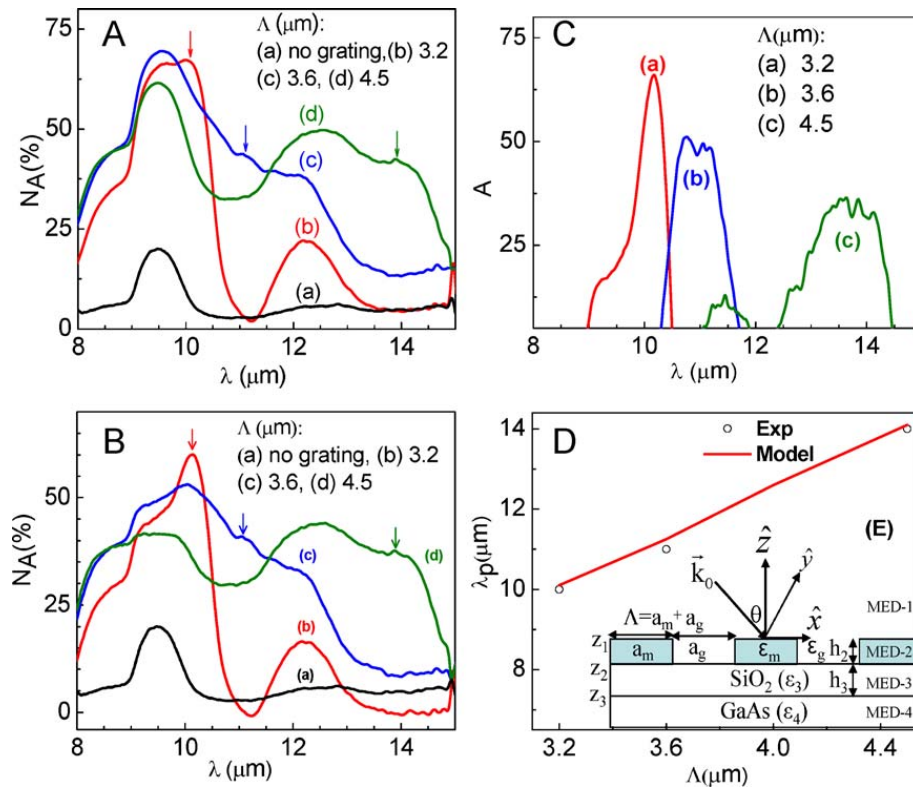
Fig. 1. (A) FTIR measured absorption for three samples with grating and one without grating. Arrows indicates the plasmonic peak position, shifting from 10 to 14 μm as Λ varies from 3.2 to 4.5 μm. (B) The data plotted after subtracting no-grating absorption from the absorption with grating, showing plasmonic peaks more clearly. (C) The data after subtracting the remaining curves from the individual curve and multiplying them by a constant factor to keep the same original peak heights. This shows plasmonic peaks more convincingly. (D) Comparison of measured and calculated absorption peak wavelength positions, showing a reasonable agreement. (E) The schematic of the structure and the coordinate system ($h_2 = 65$ nm, $h_3 = 100$ nm, $\theta = 9°$).

3. Sample fabrication

Metal grating samples with oxide layer (SiO$_2$) were fabricated on a semi-insulating GaAs wafer. The layers constituting a sample structure are schematically shown in Fig. 1(E) and are the same as discussed in Section 2. Four different samples, one having no grating (reference) and other three consisting of grating with pitch (Λ) = 3.2, 3.6, and 4.5 μm, and mark fraction[8] (a_m/Λ) = 0.5 were fabricated using standard lift-off technique. Metal grating patterns were obtained from the gold (Au) and titanium (Ti) metallization layers using electron beam lithography. The thicknesses of Au and Ti layers were kept 50 and 15-nm, respectively. Titanium (Ti), the most commonly used adhesive material to deposit gold onto dielectric/semiconductor layers, was used as an adhesive in the present case, too. The oxide layer of thickness 100-nm was deposited by plasma-enhanced chemical vapor deposition (PECVD), and the dielectric constant was measured as 2.12.

4. Results and discussion

Fourier Transform Infrared (FTIR) measurements were made on the fabricated samples. Room temperature (300 K) absorption spectra experimentally measured for sample with no grating (Fig. 1A(a)) shows two absorption bands (peaking ~λ = 9.5 and 12.2 μm) derived from the asymmetric and the symmetric stretching of Si–O–Si pairs in SiO$_2$ layer [11]. In addition to the SiO$_2$ absorption bands, the samples with grating also exhibit absorption peaks indicated by an arrow ~λ = 10 μm (Λ = 3.2 μm, Fig. 1A(b)), 11 μm (Λ = 3.6 μm, Fig. 1A(c)), and 14 μm (Λ = 4.5 μm, Fig. 1A(d)), nonexistent in the reference spectra. To improve the visibility of these peaks, limited due to their overlapping with the SiO$_2$ absorption bands, the data after subtracting no-grating absorption from the absorption with grating are presented in Fig. 1(B). Although subtraction cannot nullify the SiO$_2$ absorption features completely (grating amplifies SiO$_2$ absorption bands, too), this shows 10 μm peak clearly. To witness all grating derived peaks more convincingly, Fig. 1 data, after subtracting the remaining curves from the individual curve and multiplying them by a constant factor to keep the same original peak heights are further plotted in Fig. 1(C), showing all three peaks clearly. The comparison of measured and the calculated peak wavelengths is presented in Fig. 1(D). The agreement between the measured and the calculated peak wavelengths is reasonable, considering the facts: (i) measured samples consist of Au and Ti grating, while
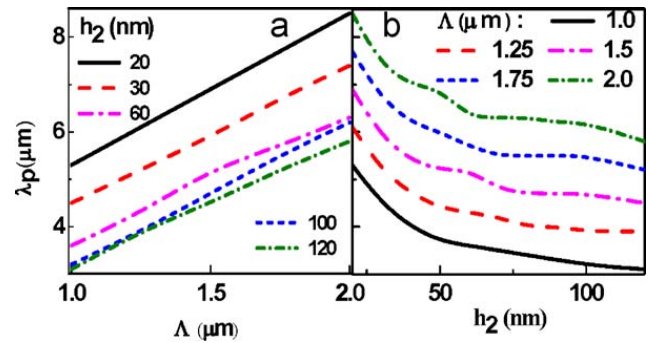
Fig. 2. The calculated variation of λ_p with: (a) grating pitch, Λ for different grating heights h_2 (h_3 = 100 nm, θ = 9°) and (b) grating height h_2 for gratings of different pitch Λ.

our model considers the grating to be made of Au, and (ii) the actual and modeled [8,10] dielectric functions may be slightly different.

Next, in order to use the plasmonic effects to improve the performance of our recently developed 3–5 μm room temperature split-off detectors [12], the role of grating parameters is theoretically-investigated (keeping structure parameters and incidence conditions the same as in the samples for comparison). The absorption peak wavelength (λ_p) red-shifts linearly with increasing Λ (see, Fig. 2a), following the relation: λ_p (μm) = $u \times \Lambda$ (μm) + c, u and c denoting the slope and the intercept, respectively. The shift is caused by the change of Brillouin zone size, resulting from the change in the magnitude of the Bragg vector K (=$m\pi/\Lambda$) with changing Λ. The change in K leads to a change in the magnitude of the SP wave vector, $k_{sp} = (\omega/c) \sin\theta + 2K$ [13] and hence, the change in the resonant wavelength, $\lambda_p = 2\pi/k_{sp}$. The effect of grating height (h_2) on λ_p, the nonlinear blue-shift with increasing h_2, is shown in Fig. 2(b). The dependence of λ_p on h_2 and Λ is in accordance with the reports for the visible region and different geometries [14,15]. The role of grating parameters in absorption (measure of coupling efficiency [16]) maximization is illustrated in Fig. 3 by a 3D plot of the spectral variation of N_A with h_2 (Λ = 1.0 μm). Evidently, N_A for a fixed λ can be varied by varying h_2 and can be maximized by using an optimum h_2 value determined from calculations. Quantitatively, for instance at λ = 4.4 μm, h_2 = 32 nm (optimum) gives $N_A(\%)$ = 67.1, while for ±10 nm change in h_2, $N_A(\%)$ reduces to 34.6 and 46.8, respectively. Similarly, at λ = 4.8 μm, h_2 = 26 nm (optimum) gives $N_A(\%)$ = 61.5, while for ±10 nm change in h_2, $N_A(\%)$ reduces to 36.8 and 24.1, respectively. The set of optimized parameters to achieve maximum absorption at 4.4 μm are Λ = 1.00 μm,
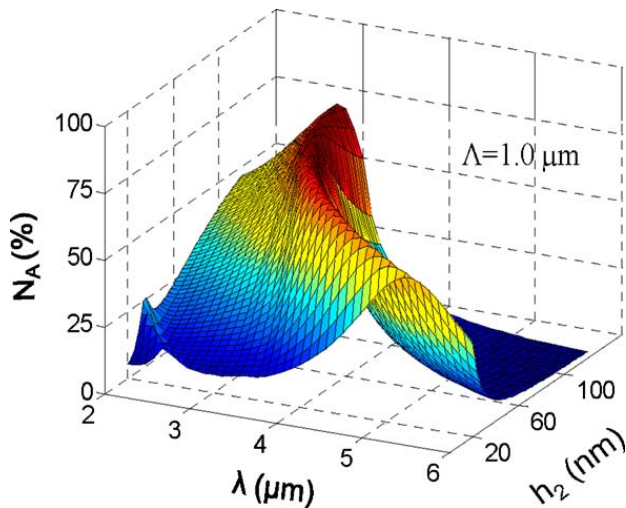
Fig. 3. The calculated variation of N_A as a function of λ and h_2 ($\Lambda = 1.0$ μm, $h_3 = 100$ nm, $\theta = 9°$). The dependence of N_A and λ_p on h_2, and the existence of optimum grating height can be visualized.
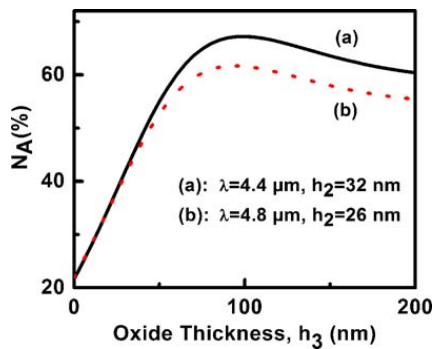
Fig. 4. The calculated effect of SiO$_2$ thickness (h_3) on optical absorption for (a) $\lambda = 4.4$ μm, $h_2 = 32$ nm (optimized grating height), and (b) $\lambda = 4.8$ μm, $h_2 = 26$ nm (optimized grating height).

$h_2 = 32$ nm, $h_3 = 100$ nm (producing, $N_A = 67.1\%$), and at 4.8 μm are $\Lambda = 1.00$ μm, $h_2 = 26$ nm, $h_3 = 100$ nm (producing, $N_A = 61.5\%$). The effect of different geometrical parameters, such as groove width, groove depth and the period on the coupling efficiency, and the tuning of resonant wavelength has also been reported for the bull's eye structure [17], which are important device elements for photodetectors, Vertical Cavity Surface Emitting lasers (VCSELs), and Quantum Cascade Lasers (QCLs). The tuning capability of resonant wavelength using geometrical parameters has also been investigated. The effects of oxide thickness on N_A for these two sets of grating heights is shown in Fig. 4. N_A increases with the oxide thickness, reaches a maximum and then decreases. Primarily the decrease may be attributed to the reduced plasmon coupling beyond certain oxide thickness, but further investigations are required. The vitality of the structure parameters for the fine tuning of λ_p and controlling
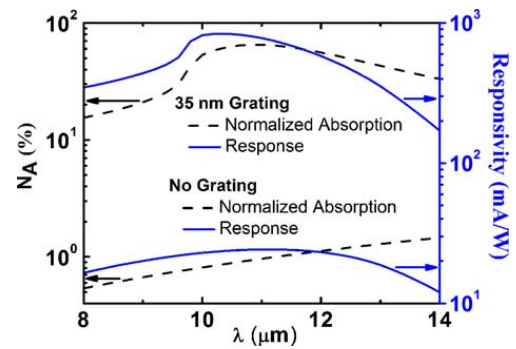
Fig. 5. The calculated responsivity and normalized absorption for a typical GaAs/AlGaAs heterostructure with a 35-nm grating and without grating. Other parameters are $\Lambda = 3.0$ μm, GaAs thickness = 100 nm, doping = 1×10^{19} cm^{-3}, Al = 0.12 and $\theta = 1°$.

the absorption efficiency is significant from the fabrication point of view, as it suggests that the precise control of fabrication processes is imperative.

Finally, a metallic grating for augmenting FCA and plasmonic absorption in a typical HEIWIP structure consisting of a metallic grating at the top, followed by p-doped GaAs and undoped Al$_{0.12}$Ga$_{0.88}$As layers is theoretically optimized for maximum response in the mid-infra red region ($\lambda_{\text{peak}} \sim 10$ μm). The optimized parameters are $h_2 = 35$ nm and $\Lambda = 3.0$ μm. The calculated normalized absorption with optimized grating antenna and also without grating antenna are shown in Fig. 5. Estimated responsivity $R(=q\eta\lambda/hc)$, η being the quantum efficiency, and other symbols have their usual meaning) [18] for both cases (with and without grating mediated absorption) are also shown in Fig. 5. Remarkably, a substantial absorption and responsivity improvement in the IR region can be realized by integrating an optimized metallic antenna with HEIWIP structures. Performance improvements using surface plasmon enhancement has recently been demonstrated for InAs Quantum Dot (QD) based photodetectors [19,20]. The present results on the resonant wavelength tuning through geometrical parameters for the HEIWIP structures are supported by similar results reported for QD-based photodetectors [20]. An important advantage of using plasmonic effects is the near field enhancement of the electric field. This is shown in Fig. 6, where electric field intensity $|E_z|^2$ as a function of the distance from the metal-dielectric interface is plotted for $h_2 = 35$ nm, $\Lambda = 3.0$ μm, and $\lambda = 10$ μm. In the figure, the shaded part indicates the region of existence of a strong electric field, which decays exponentially with the distance from the metal-dielectric interface as anticipated for the surface confined waves. The implementation of plasmonic enhancement requires placement of the device active
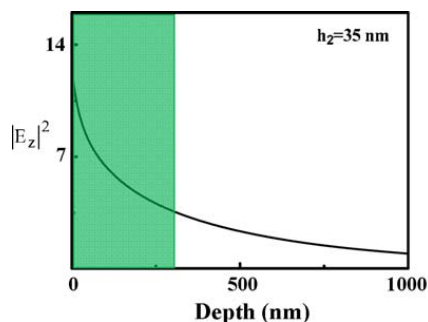
Fig. 6. The calculated variation of the electric field intensity $|E_z|^2$ as a function of the distance from the metal/dielectric interface for $h_2 = 35$ nm, $\Lambda = 3.0$ μm, and $\lambda = 10$ μm. Noticeably, the strong field exists up to about 300 nm (shown by the shaded region). This shows the practicability of the proposed approach for these structures. Other parameters are GaAs thickness = 100 nm, doping = 1×10^{19} cm^{-3}, and Al fraction = 0.12.

region within the penetration depth, about 300 nm, so the strong overlap of the optical field with the active region can occur. This situation is ideally suited for the HEIWIP structure, where typical effective active region thickness after etching is approximately 100 nm and the active region can be positioned immediately next to the plasmonic element. Moreover, the required feature sizes (∼μm) for mid-infrared region can be obtained using photolithography rather than comparatively expensive e-beam lithography that must be used for the visible region. As a further advantage, the integration of a plasmonic element with photodetectors has recently been shown not to degrade the photodetector speed [20,21]. Therefore, the advantages of conventional designs remain valid in the plasmonic version, too.

5. Conclusions

In summary, metallic corrugation-induced IR absorption is experimentally demonstrated and theoretically corroborated. Integration of optimized metallic corrugation with a typical HEIWIP structure is shown to improve their performance. The vitality of grating parameters in performance optimization is described.

Acknowledgments

References

[1] M.I. Stockman, Slow propagation, anomalous absorption, and total external reflection of surface plasmon polaritons in nano-layer systems, Nano Lett. 6 (2006) 2604–2608.

[2] A.P. Hibbins, W.A. Murray, J. Tyler, S. Wedge, W.L. Barnes, J.R. Sambles, Resonant absorption of electromagnetic fields by surface plasmons buried in a multilayered plasmonic nanostructure, Phys. Rev. B 74 (1–4) (2006) 073408.

[3] G. Leveque, O.J.F. Martin, Optimization of finite diffraction gratings for the excitation of surface plasmons, J. Appl. Phys. 100 (1–6) (2006) 124301.

[4] J. Lu, C. Petre, E. Yablonovitch, J. Conway, Numerical optimization of a grating coupler for the efficient excitation of surface plasmons at an Ag–SiO$_2$ interface, J. Opt. Soc. Am. B 24 (2007) 2268–2272.

[5] Z. Yu, G. Veronis, S. Fan, M.L. Brongersma, Design of mid-infrared photodetectors enhanced by surface plasmons on grating structures, Appl. Phys. Lett. 89 (1–3) (2006) 151116.

[6] E. Dupont, Optimization of lamellar gratings for quantum-well infrared photodetectors, J. Appl. Phys. 88 (2000) 2687–2692.

[7] G. Tayeb, R. Petit, On the numerical study of deep conducting lamellar diffraction gratings, Opt. Act. 31 (1984) 1361–1365.

[8] L. Wendler, T. Kraft, Theory of grating-coupler-assisted infrared spectroscopy of lower-dimensional electron systems: local optics of anisotropic multilayer systems with grating, Phys. B: Condens. Matter 271 (1999) 33–98.

[9] A.G.U. Perera, G. Ariyawansa, P.V.V. Jayaweera, S.G. Matsik, M. Buchanan, H.C. Liu, Semiconductor terahertz detectors and absorption enhancement using plasmons, Microelectron. J. 39 (2008) 601–606.

[10] P. Hewageegana, V. Apalkov, Quantum dot photodetectors with metallic diffraction grating: surface plasmons and strong absorption enhancement, Phys. E: Low-dimens. Syst. Nanostruct. 40 (2008) 2817–2822.

[11] S.M. Han, E.S. Aydil, Detection of combinative infrared absorption bands in thin silicon dioxide films, Appl. Phys. Lett. 70 (1997) 3269–3271.

[12] A.G.U. Perera, S.G. Matsik, P.V.V. Jayaweera, K. Tennakone, H.C. Liu, M. Buchanan, G. Von Winckel, A. Stintz, S. Krishna, High operating temperature split-off band infrared detectors, Appl. Phys. Lett. 89 (1–3) (2006) 131118.

[13] N. Félidj, J. Aubard, G. Lévi, J.R. Krenn, G. Schider, A. Leitner, F.R. Aussenegg, Enhanced substrate-induced coupling in two-dimensional gold nanoparticle arrays, Phys. Rev. B 66 (1–7) (2002) 245407.

[14] G. Leveque, O.J.F. Martin, Numerical study and optimization of a diffraction grating for surface plasmon excitation, Proc. SPIE 5927 (1–9) (2005) 592713.

[15] J. Cesario, R. Quidant, G. Badenes, S. Enoch, Electromagnetic coupling between a metal nanoparticle grating and a metallic surface, Opt. Lett. 30 (2005) 3404–3406.

[16] Z. Chen, I.R. Hooper, J.R. Sambles, Strongly coupled surface plasmons on thin shallow metallic gratings, Phys. Rev. B 77 (1–4) (2008) 161405.

[17] O. Mahboub, S.C. Palacios, C. Genet, F.J. Garcia-Vidal, S.G. Rodrigo, L. Martin-Moreno, T.W. Ebbesen, Optimization of

bull's eye structures for transmission enhancement, Opt. Exp. 18 (2010) 11292–11299.

[18] D.G. Esaev, M.B.M. Rinzan, S.G. Matsik, A.G.U. Perera, Design and optimization of GaAs/AlGaAs heterojunction infrared detectors, J. Appl. Phys. 96 (2004) 4588–4597.

[19] J. Rosenberg, R.V. Shenoi, T.E. Vandervelde, S. Krishna, O. Painter, A multispectral and polarization-selective surface-plasmon resonant mid-infrared detector, Appl. Phys. Lett. 96 (2009) 161101.

[20] C.C. Chang, Y.D. Sharma, Y.S. Kim, J.A. Bur, R.V. Shenoi, S. Krishna, D. Huang, S.Y. Lin, A surface plasmon enhanced infrared photodetector based on InAs quantum dots, Nano Lett. 10 (2010) 1704–1709.

[21] J.A. Shackleford, R. Grote, M. Currie, J.E. Spainer, B. Nabet, Integrated plasmonic lens photodetector, Appl. Phys. Lett. 94 (2009) 083501.